NATIONAL RADIO ASTRONOMY OBSERVATORY
Green Bank, West Virginia

ELECTRONICS DIVISION INTERNAL REPORT NO. 297

CHARACTERIZATION AND OPTIMIZATION OF THE NRAO/BALZER'S
THREE STAGE CLOSED CYCLE JT REFRIGERATOR

D. Schroeter, J. Lamb

November 1994

Characterization and Optimization of the NRAO / Balzer's

Three Stage Closed Cycle JT Refrigerator

D. Schroeter[1], J. Lamb[2]

[1]Reed College, Portland, OR 97202
[2]National Radio Astronomy Observatory, Tucson, AZ 85719

Abstract

The NRAO 1W Joule-Thompson refrigerator has been installed and tested on a Model UCH 130 refrigerator which precools the third stage. The Balzers Model UCH 130 refrigerator is a two stage closed cycle refrigerator which works on the Gifford-McMahon cycle. The NRAO/Balzers refrigerator was found to be able to sustain third stage loads of up to 2200 mW with no load on the first or second stages, and up to 1500 mW with a 50 W load on the first stage, and a 2 W load on the second stage. The refrigerator has advantages over previous designs in its increased load capacity, which should make for less expensive operating costs.

1. Introduction

The National Radio Astronomy Observatory (NRAO) has been using 1 W Joule-Thompson refrigerators which incorporate the CTI 1020 refrigerator to precool the 3rd stage. The purpose of this report is to examine the performance of such refrigerators when a Balzers Model UCH 130 refrigerator is used instead of the CTI unit. We obtained experimental data for the holding and cooling capacities of the refrigerator. In addition we tested the effects of varying JT pressure, GM pressure, GM cycle frequency, and the heat load on both the 1st and 2nd stages. This data is compared with theoretical models when applicable. Finally, a theoretical treatment was given to the conduction through the hydrogen heat switch, conduction in the JT structure, and radiative loading.

2. Fundamentals of Refrigerator Operation

The NRAO/Balzers refrigerator uses the Joule-Thompson effect to cool the 3rd stage. In a true free expansion process, no work is done and the internal energy of the system, U, remains constant. In the case of the Joule-Thompson effect, an amount of gas, n moles, at initial pressure and volume (p_1, V_1) is passed through a small aperture to a final pressure and volume (p_2, V_2). The internal energy of the system changes by the amount of work done by the gas so that

$$(2.1) \qquad U_2 - U_1 = p_1V_1 - p_2V_2$$

In this case, it is not the internal energy, but the enthalpy, defined as

$$(2.2) \qquad H = U + pV$$

which remains conserved. Such a process, in which enthalpy is conserved, is called isenthalpic. Enthalpy can be thought of as the amount of heat that one would need to remove from a system in order to bring the temperature to absolute zero, and is a function of both temperature and pressure. Isenthalps for helium gas are shown in Fig. 2.1.

Fig. 2.1 Isenthalpic Curves for Helium Gas[1]
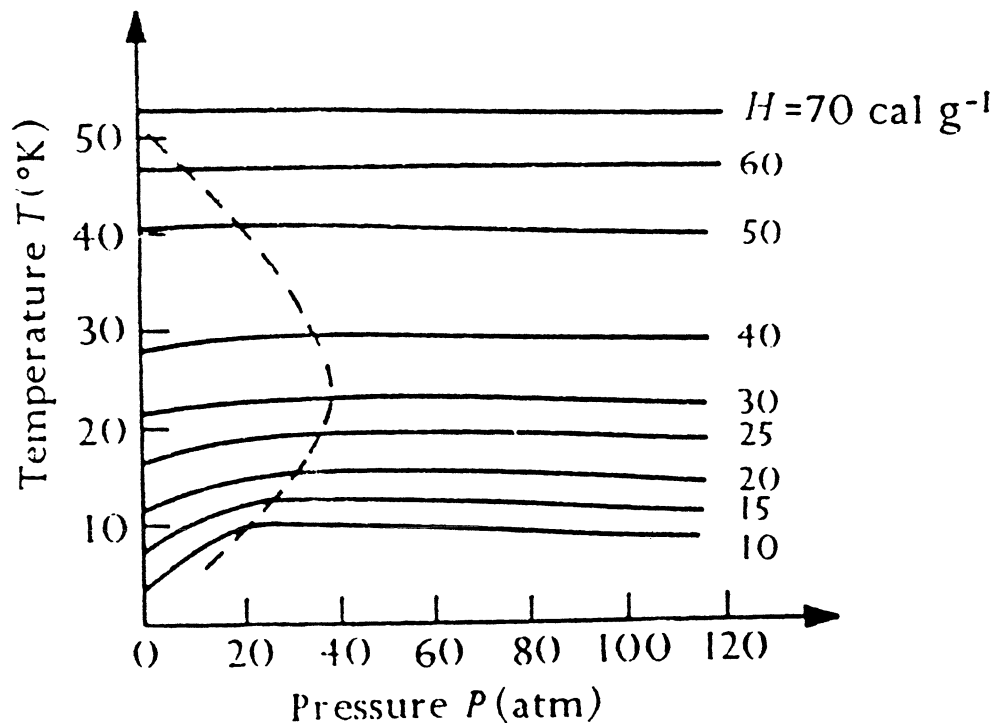
1. taken from G. K. White, Experimental Techniques in Low Temperature Physics, 1968, p. 5.

It is clear that if an initial pressure, p_1, is chosen which lies to the left of the dashed curve in Fig. 2.1, expansion to a lower pressure, p_2, along one of the isenthalps will result in a lower temperature for the system. Since our JT valve is normally run with an input pressure, p_1, of 19 atm (1390 kPa), we see that the temperature must be reduced to at least 40 K in order for the process to produce cooling. This is why we must use a pre-cooler such as the Balzers Model UCH 130 refrigerator with our JT valve (see below).

The process works because of intermolecular attractions between molecules in the gas. The kinetic energy of the gas molecules, K, given by

$$(2.3) \qquad\qquad\qquad K = 1/2 \, mv^2 = 3/2 \, kT$$

where m is mass, v is velocity, k is the Boltzmann constant, and T is temperature, becomes very small at low temperatures. In this region, the intermolecular attractions become significant. Since transferring the gas from high to low pressure requires the mean separation between molecules to increase, it takes energy to pull them apart, and this provides the cooling. The effect will not work for an ideal gas, as the ideal gas law assumes no attraction between molecules.

The refrigerator incorporates a Balzers Model UCH 130 Refrigerator to precool the gas for the JT. The Balzers UCH Model 130 Refrigerator is a two stage closed cycle refrigerator, using the Gifford-McMahon (GM) thermodynamic cycle. It consists of a single piston containing two regenerator matrices. The cylinder starts at the bottom of its swing (Fig. 2.2), with the high pressure valve open. The cylinder is then moved to the top of its swing, causing the gas to flow through the regenerator matrices. The gas volumes are filled with high-pressure gas by the compressor. As a side effect, the gas is heated while it is in the compressor. This heat is mainly dissipated before the regenerators and the gas flows through the piston, emerging in the volumes at ambient temperature. With the cylinder still at the top of its swing, the high pressure valve is closed and the low pressure valve is opened. This causes the gas to expand and this expansion comes at the expense of heat, cooling the gas and the two stages adjacent to the gas volumes. The cylinder is then returned to the bottom of its swing, forcing the gas remaining in the volumes through the regenerator, and cooling the regenerator back down. On subsequent cycles the gas is cooled further by the regenerator until a low-temperature equilibrium is achieved. The cycle is repeated at anywhere from 56 - 144 rpm.

Fig. 2.2 Schematic of Gifford-McMahon Refrigerator
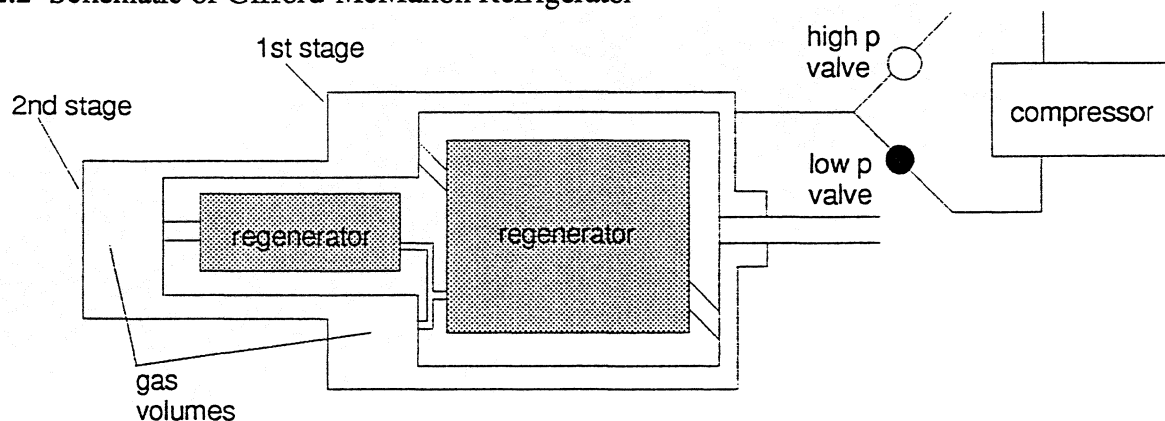
3. Refrigerator Load Capacity

The refrigerator will be subject to a number of heat loads when used in a receiver. These loads include, but are not limited to, radiative loads, conduction loads through cables, supports, and waveguides, as well as the loads which the refrigerator is subject to in the lab (see "5. Refrigerator Loading"). It is not the purpose of this report to give a quantitative treatment of these various heat loads[1]. We make the assumption that our refrigerator will be subject to a load of no more than 50 W on the 1st stage and 2 W on the second stage, in addition to any load which is present in the laboratory dewar.

We tested the refrigerator capacity by applying different heat loads to the 1st and 2nd stages, and a variable heat load on the 3rd stage. We define the "holding capacity" as the greatest heat load which may be applied to the 3rd stage without the 3rd stage temperature exceeding 5K, and the "cooling capacity" as the power to which the heat load on the 3rd stage must be reduced so that the 3rd stage temperature will again drop below 5 K. We ran four trials: one with no loading on either stage, one with 2 W on the 2nd stage only, one with 50 W on the 1st stage only, and one with 2 W on the 2nd stage and 50 W on the 1st stage (Fig. 3.1). These tests were performed with a JT input pressure of 1930 kPa, a GM input pressure of 2070 kPa and a cycle frequency of 144 rpm.

Fig. 3.1 Load Test with Variable 1st and 2nd Stage Loading
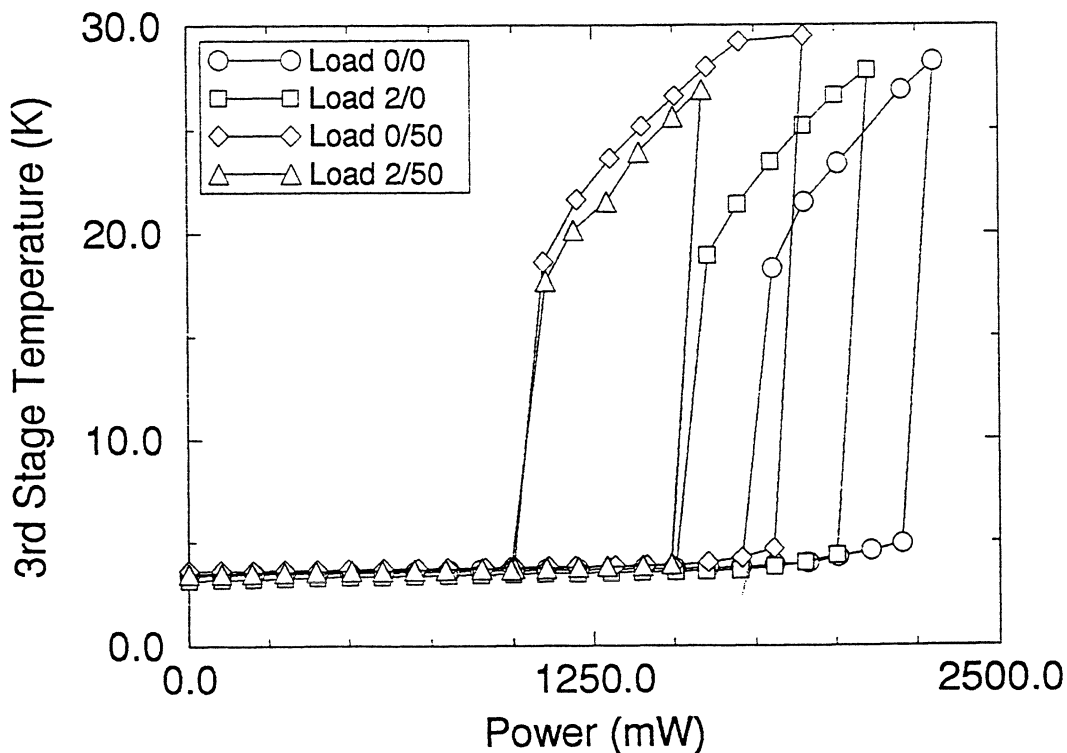
1. for such a treatment see J.R. Fisher, *Typical Heat Loads in a Cryogenic Dewar and a Discussion of the Refrigerator Principles of Operation*, 1979, p. 11-25.

We can learn quite a bit from the shape of the curve in Fig. 3.1. As the helium pot is located on the low pressure end of the JT valve (Fig. 3.2), there is already a mixture of helium gas and liquid at this point in the JT circuit. As long as there is helium liquid, any heat applied to the 3rd stage will go to vaporizing this liquid, resulting in no net increase in temperature. Therefore, the slope of the linear region in Fig. 3.1 (see detail in Fig. 3.3) is a measure of the thermal resistance of the medium between the temperature sensor and the helium in the JT circuit. For our data we obtained a mean value of 0.23 W/K for this thermal resistance, with a standard deviation of 0.04. This value is approximately the resistance of a cube of OFHC Cu (from which the 3rd stage is constructed) 1 cm on a side. The variation in the four values is small and could be attributed to thermometer placement or variations in the mass flow rate in the JT circuit.
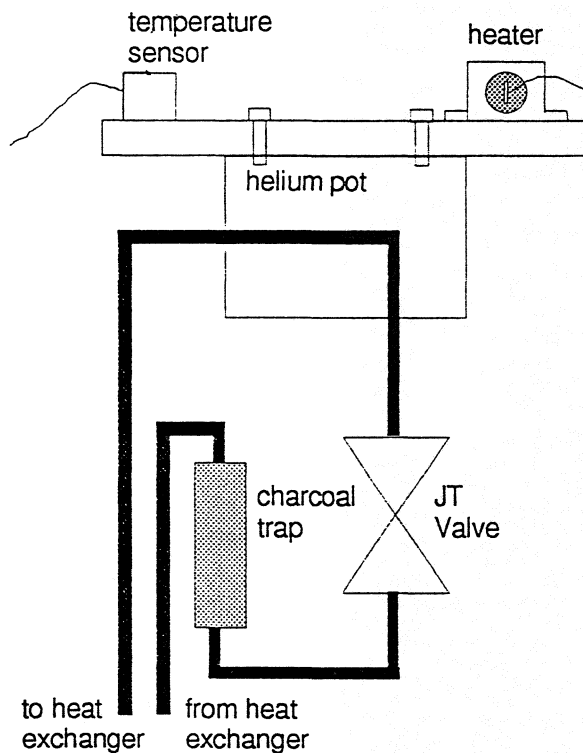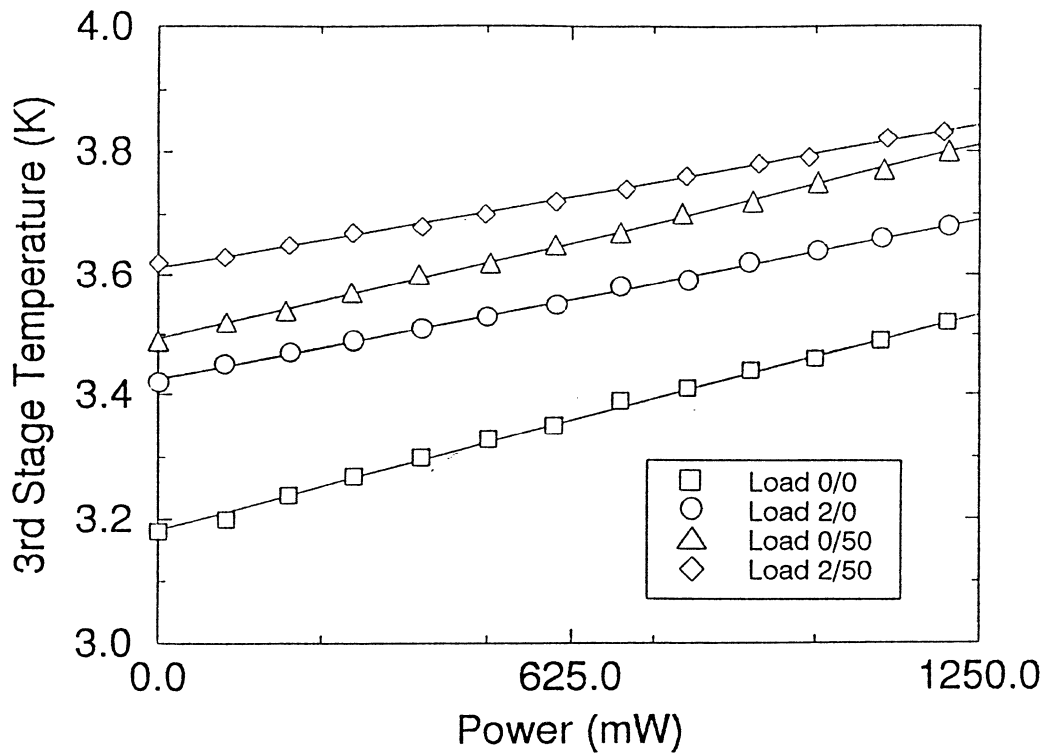
Fig. 3.2 Third Stage Detail

Fig. 3.3 Detail of Fig. 3.1

The amount of helium liquid in the circuit decreases (Fig. 3.4) until the holding capacity is reached. At this point all of the liquid helium has been evaporated and the heat applied to the 3rd stage must now go into warming the gas, causing a dramatic rise in temperature. Since the Joule-Thompson effect is most efficient at low temperatures (see "2. Fundamentals of Refrigerator Operation"), the refrigerator must bootstrap its way back down to full operation. The point at which the heat flow on the 3rd stage is low enough to allow this is the "cooling capacity".

Fig. 3.4 Detail of Fig. 3.1
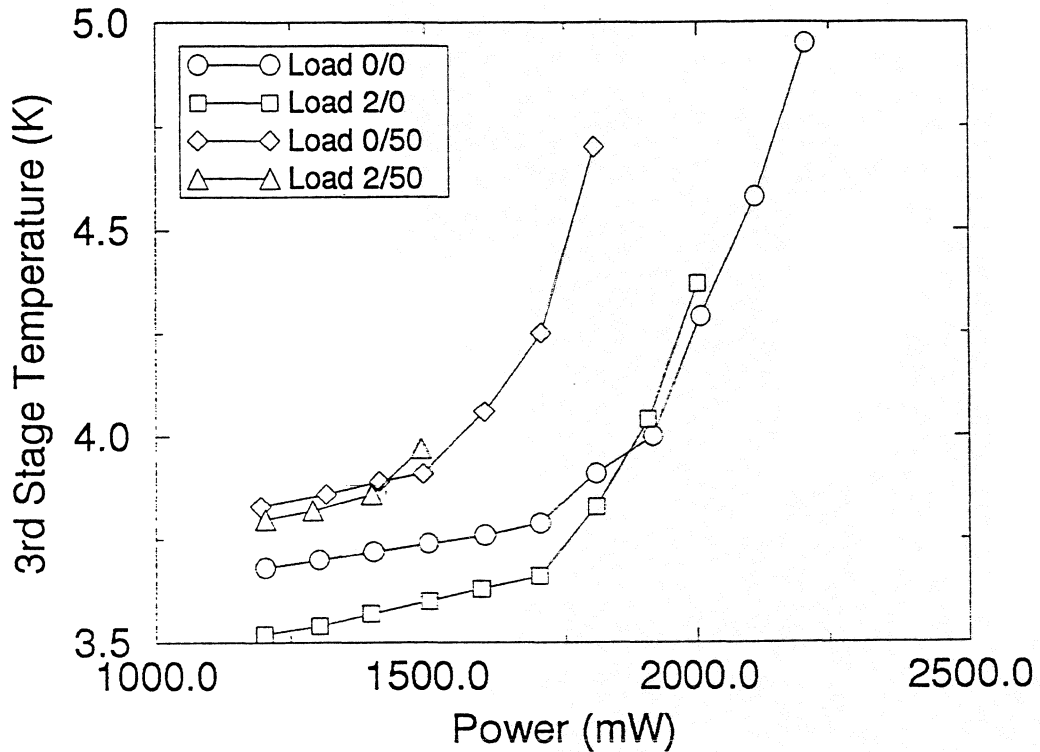
The findings of this set of experiments, including thermal resistance, holding and cooling capacity, are shown in Fig. 3.5. Note that even with a load of 50 W on the 1st stage and 2 W on the 2nd stage, we are achieving a holding capacity of 1592 mW. This is substantially larger than the 1000 mW which our refrigerator will be subject to during operation.

Fig. 3.5 Refrigerator Characteristics

| 1st Stage Load (W)	2nd Stage Load (W)	Thermal Resistance (K/W)	Holding Capacity (mW)	Cooling Capacity (mW)
0	0	0.21	2307	1704
0	2	0.25	2102	1504
50	0	0.18	1906	1002
50	2	0.28	1592	994

4. Analysis of JT Circuit

Fig 4.1 shows three experimental runs obtained at 3 different JT input pressures. We see that the input pressure to the JT valve is important in determining the refrigerator's capacity. The presence of liquid in the JT circuit means that the refrigerator can handle a heat load equal to the amount of liquid times its latent heat of evaporation. When there is no more liquid present in the circuit we see that the temperature skyrockets (point marked "b" in Fig. 4.4) as the heat dissipated by the circuit must now go into warming the gas in the circuit and not evaporating liquid. The latent heat of evaporation, H_L, is the amount of energy required to enact a phase change from liquid to gas for a specified amount of a substance, in our case the gas is helium which has an H_L of 82.4 J/mol. We know the mass flow rate, Δm, through the circuit, and the percentage of this gas which is liquefied is given by[1]

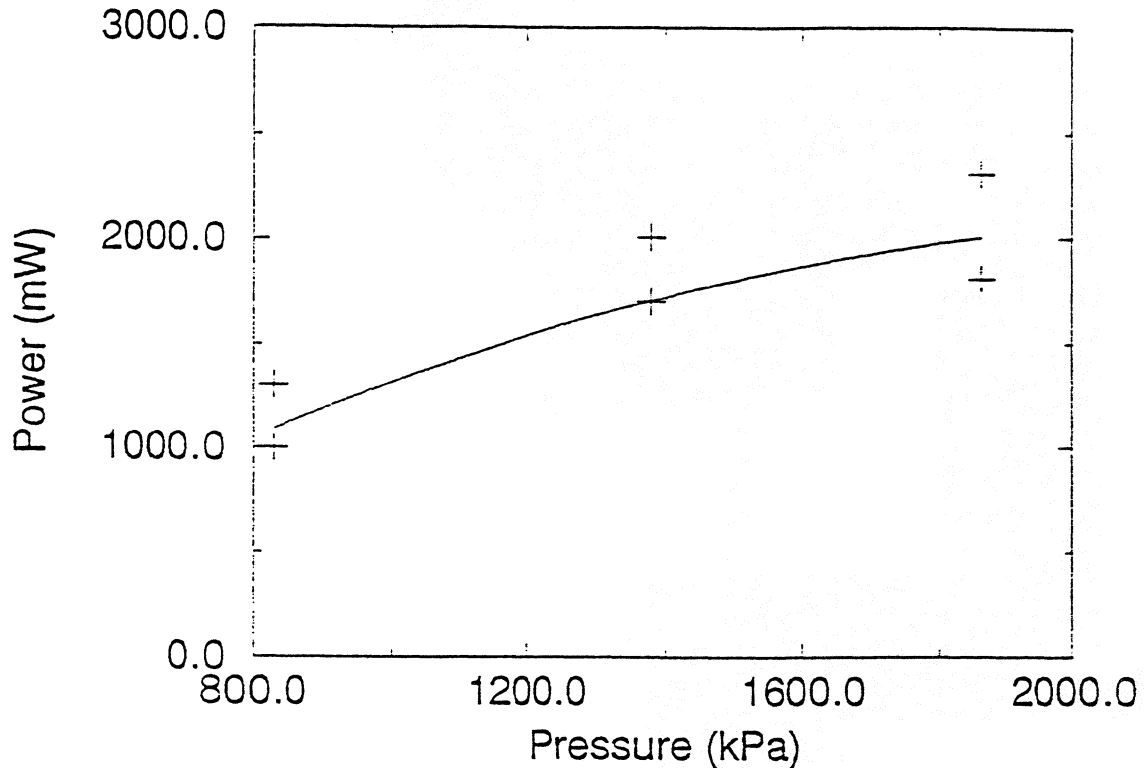(4.1)   % liquefied = $(H_2-H_1)/(H_2-H_L)$

where H_2 is the enthalpy of the gas on the output side of the warm end of the 3rd stage heat exchanger, and H_1 is the enthalpy of the gas on the input side of the warm end of the heat exchanger.

Fig. 4.1 Variable JT Pressure Load Test
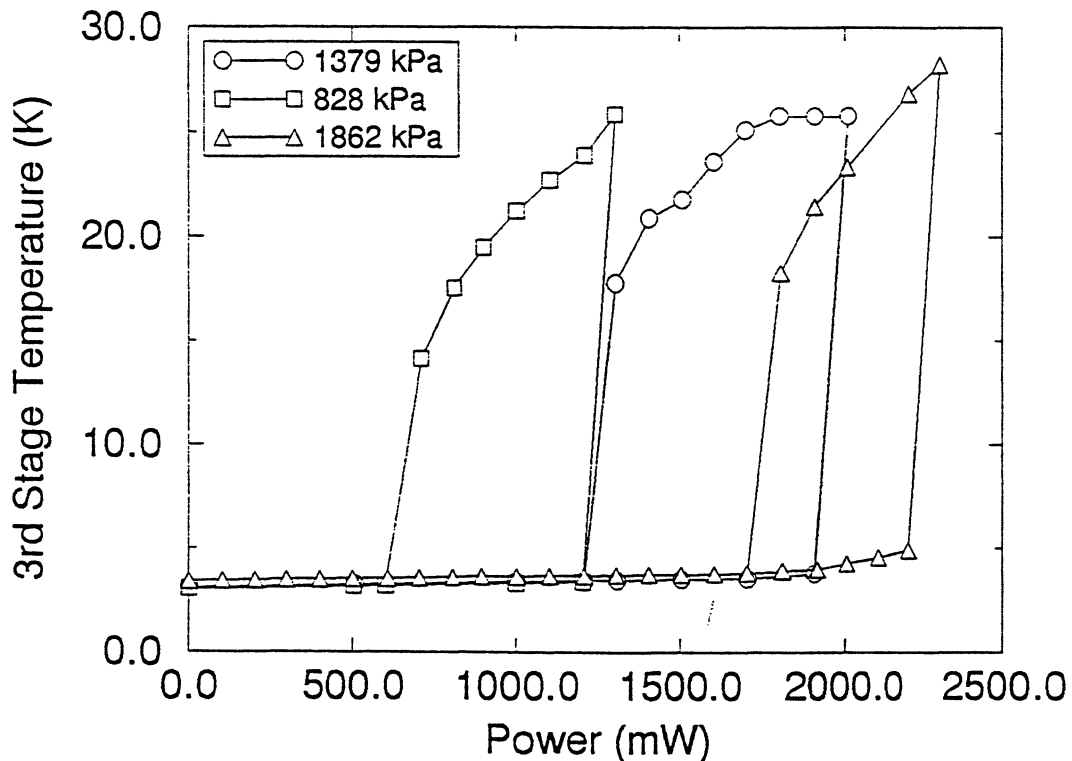
1. G. K. White, Experimental Techniques in Low-Temperature Physics, 1968, p. 7.

Fig. 4.2 Detail of Variable JT Pressure Load Test

The capacity of the refrigerator, P, is then given by

(4.2) $$P = \Delta m \; H_L \; (H_2\text{-}H_1)/(H_2\text{-}H_L)$$

where the quantities are as listed above. Using tabulated data[2] for the enthalpy of gaseous He, we can evaluate this expression as a function of pressure. We used the 2nd stage temperature, flow rate, and output pressure associated with the experimental runs at 828, 1379, and 1862 kPa (shown in Fig. 4.1) in evaluating this expression (see Fig. 4.3). The range in the column marked "Experimental Power" is the range between points "a" and "b" in Fig. 4.4.

Fig. 4.3 Data for Refrigerator Capacity

Input Pressure (kPa)	Output Pressure (kPa)	Flow Rate (mol/s)	2nd Stage Temperature (K)	Theoretical Power (mW)	Experimental Power (mW)
828	48	.031	8.73	1091	1008-1300
1379	55	.038	8.83	1706	1705-2010
1862	34	.041	8.58	2006	1808-2307

A curve extrapolated from this theoretical data is shown along with experimental points taken from the beginning and end of the curved regions in a load-temperature diagram (Fig. 4.4). The fact that the theoretical data lies in between these two points indicates that, in this region, all of the helium liquid has boiled away, and we are beginning to heat up the gas.

2. Hoare, Jackson, and Kurti. Experimental Cryophysics, 1961.

Fig. 4.4 Refrigerator Load Capacity
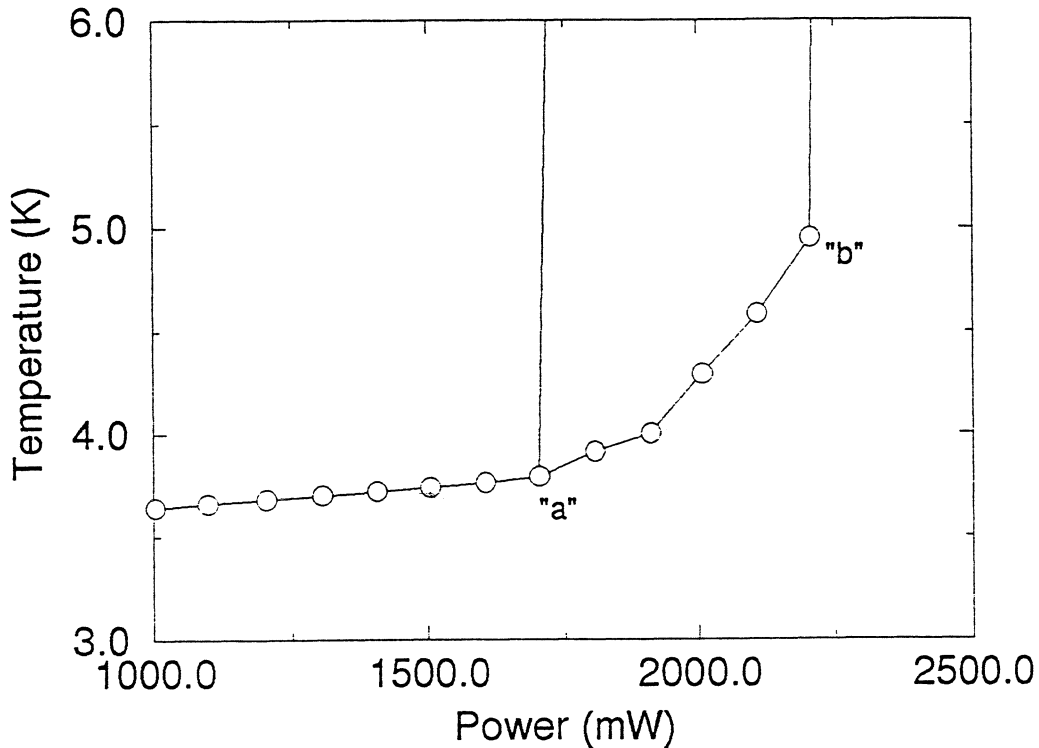
What we would like to do now is find out whether or not there is any way to improve upon this refrigerator capacity. Referring to eqn.. 4.2, we see that we would like to make the mass flow rate, Δm, as large as possible, the quantity (H_2-H_1) as large as possible, and the quantity (H_2-H_L) as small as possible. It is clear that we would like to make H_1 as small as possible, and we have no control over H_L, but the question is whether we want to make H_2 large or small. While H_L has a constant value of 82.4 J/mole, we find that H_1 ranges from 144.9 to 171.4 J/mole over the parameter space we investigated. Since H_1 is always larger than H_L, increasing the value of H_2 will have the effect of increasing the value of the fraction $(H_2-H_1)/(H_2-H_L)$, and so is desirable. There are two ways to change the enthalpy of the gas. The first is by altering its pressure, and the second by altering the temperature.

We know that enthalpy must increases monotonically with increasing temperature as enthalpy can be thought of as the amount of heat that would need to be removed from a substance to bring its temperature to absolute zero. We would therefore like to lower the temperature of H_1, thus lowering its enthalpy. This is achieved by lowering the temperature of the 2nd stage on the refrigerator. Of course this would also lower the value of H_2 by an approximately equal amount. The quantity H_2-H_1 would remain practically the same (decreasing slightly at 1862 kPa, and increasing slightly at 1379 kPa). However, the quantity (H_2-H_L) will decrease to give an overall gain in refrigerator capacity. These predictions are shown in Fig. 4.5 for 828, 1379, and 1862 kPa isobars.

Fig. 4.5 Variation of Refrigerator Capacity with Temperature
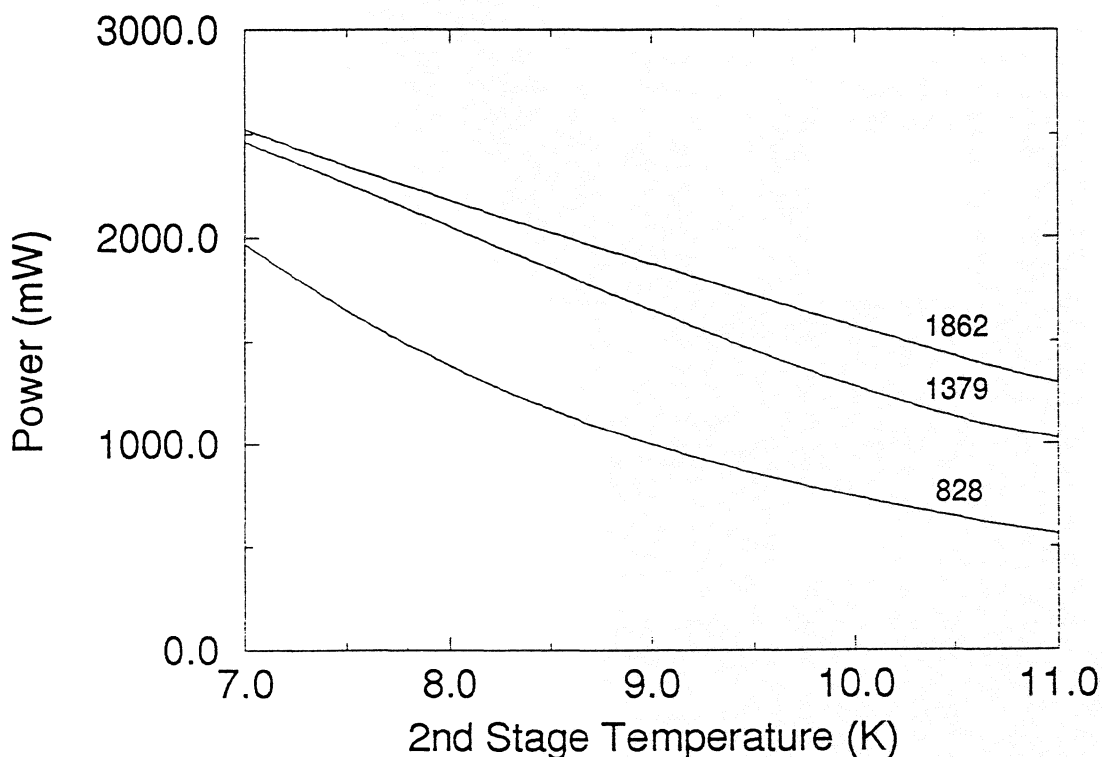
We see that the capacity of the refrigerator increases with decreasing temperature as expected and that at the lower temperatures (~7K), approximately equal results could be achieved while lowering the input pressure by 500 kPa. The dependance of the refrigerator performance on pressure is a much more complicated issue. The dependance of enthalpy on pressure is shown in Fig. 4.6. On this chart the vertical dotted lines are isobars at 45 and 1825 kPa, and the curves are isotherms from 7K to 11K. We see from the region surrounding the 45 kPa isobar that one way to increase the value of H_2 is to decrease the pressure of the return gas no matter what temperature we are at. However, the minimum return pressure is governed by the flow rate through the JT circuit and cannot be lowered below ~45 kPa at a flow rate of .037 mol/s. To see whether or not it is advantageous to raise the value of H_2 at the cost of lowering the mass flow rate, we substitute values of $\Delta m = 0.016$ mol/s, $p_R = 25$ kPa, $T_2 = 8.73$ K, and $p_I = 828$ kPa into eqn. X.2. This yields a value of 554 mW, a mere 51% of the capacity obtained with Δm and p_R at twice these values, and the other quantities held the same. Therefore it is not advantageous to lower the mass flow rate in order to achieve a lower return pressure.

Fig. 4.6 Enthalpy as a function of Pressure
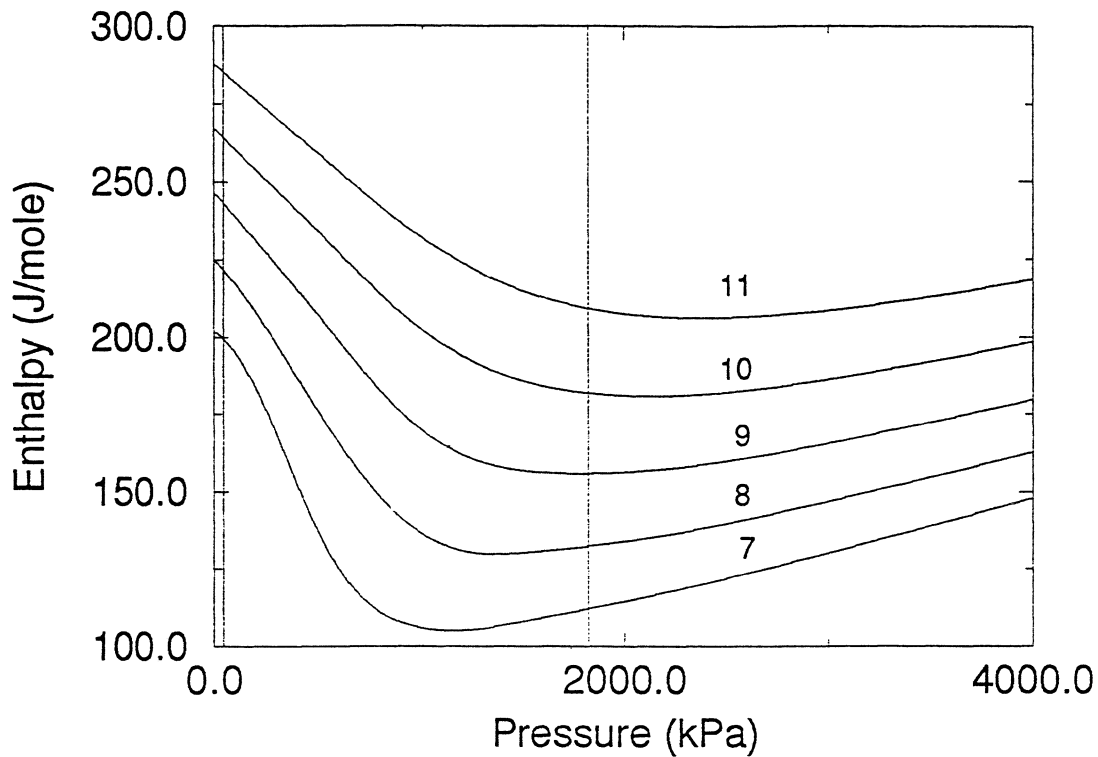
As for the input pressure we see that the 8 and 9K isenthalps are relatively flat in the region around the 1825 kPa isobar. This means that changing the input pressure will have very little effect on the value of H_1. Since mass flow is also dependent on the input temperature, we would like to keep the input pressure as high as possible. A practical working limit appears to be at about 1900 kPa.

In summary, we have found that the lower the 2nd stage temperature the better, and if the 2nd stage temperature can be reduced to about 7K, we will be able to lower the input pressure on the JT valve without a substantial loss of efficiency. We also found that we would like to make the return pressure on the JT valve as low as possible, but that it is not worth lowering it if it means a loss in mass flow rate. In addition it is very important to keep the input pressure high in order to maximize the mass flow rate. One final consideration is the efficiency of the 3rd stage heat exchanger. The above theoretical curves were derived assuming an efficiency of 1. In practice, this is impossible to achieve and a better estimate for our heat exchanger may be 0.95. The drop in the enthalpy H_2 due to the inefficiency of the heat exchanger is given by[3]

(4.3) $\Delta H = (1 - E)(H_2 - H_3)$

where ΔH is the drop in enthalpy and H_3 is the enthalpy at the input to the cool end of the heat exchanger. H_3 is at 3.5 K, the same temperature as the 3rd stage, and the enthalpy at this temperature is nearly independent of pressure, with a value of 121.3 J/mol. Substituting these values into eqn. X.3 we find an average drop of 5.8 J/mol in the enthalpy of H_2. This corresponds to an average decrease in refrigerator capacity of 5% when substituted into eqn. 4.2. If we assume an efficiency of 0.80, we obtain an average decrease in refrigerator capacity of 17%.

3. J. R. Fisher, *Typical Heat Loads in a Cryogenic Receiver Dewar and a Discussion of the Refrigerator Principles of Operation*, 1979, p. 46.

5. Refrigerator Loading

We can see what kind of load we are introducing on the first and second stages of our refrigerator by looking at a Balzers Model UCH 130 refrigerator capacity map. We plotted two points on a capacity map, one with the refrigerator in normal operation with a pressure of 1720 on the refrigerator input and the second with the JT valve turned off (Fig. 5.1). We see (from the difference between these two points) that gas conduction in the JT circuit is responsible for a load of approximately 2W on the 1st stage and 1 W on the 2nd stage. With the JT valve turned off we see that there is still a load of approximately 20 W on the 1st stage and 2 W on the 2nd stage.

Fig. 5.1 Refrigerator Capacity Map
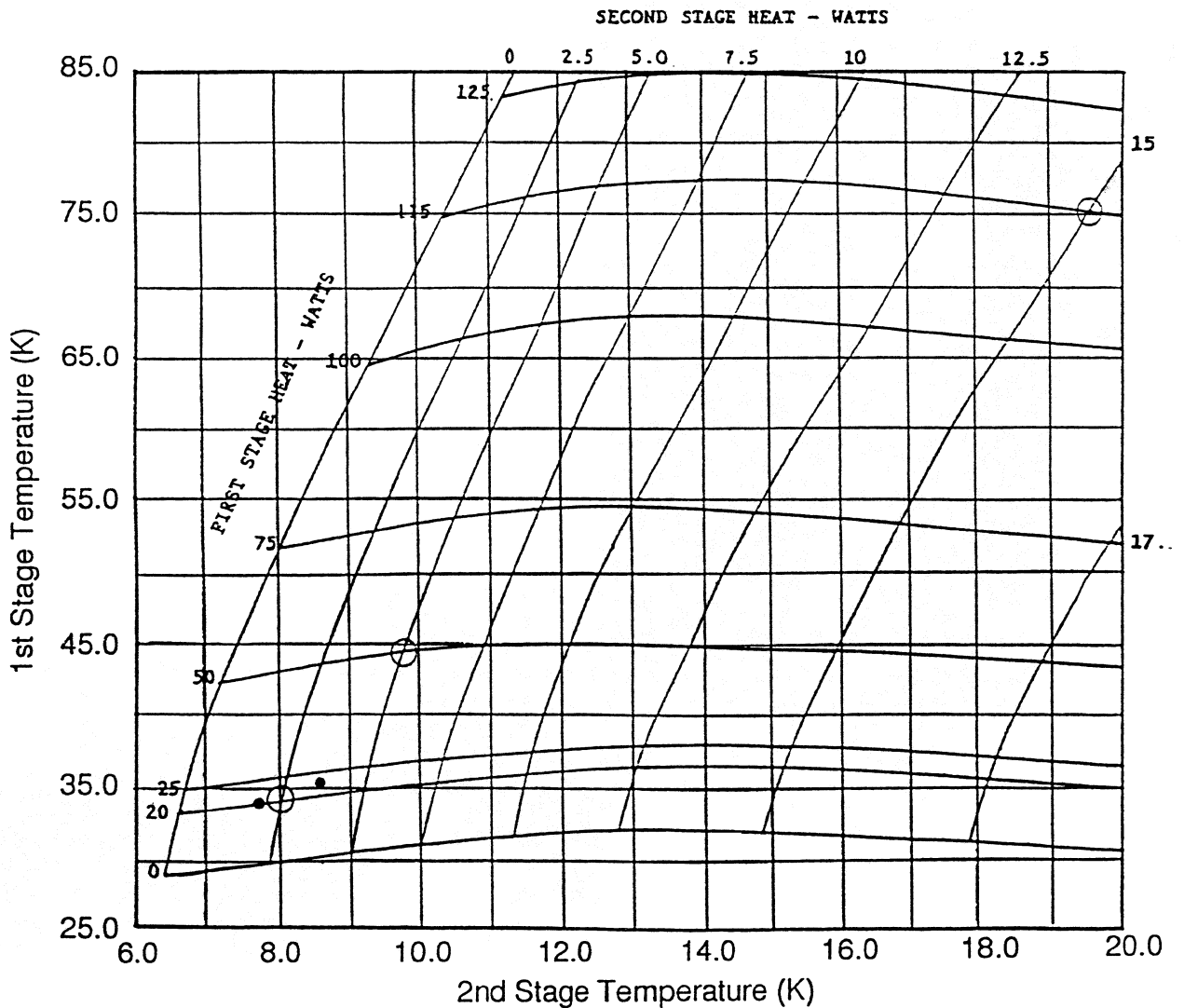
The loading seen with the JT off may be attributed to radiative loading, conduction along leads,

gaseous conduction loading in the dewar, and conduction along the JT structure and through the heat exchangers. We turn our attention first of all to radiative loading. The heat shield in the dewar is attached to the 1st stage and so all of the load incident upon the heat shield will be felt by this stage. Heat flow due to radiation is given by[1]

$$\text{(5.1)} \qquad dQ/dt = \sigma \; A \; E_{\text{eff}} \, (T_h^4 - T_c^4)$$

where σ is the Stefan-Boltzmann constant equal to 5.67×10^{-8} W/m^{2}K, A is the area of the hot surface, T_h and T_c are the hot and cold temperatures respectively, and E_{eff} is the effective emissivity which is given by[2]

$$\text{(5.2)} \qquad E_{\text{eff}} = (E_1 E_2)/(E_1 + E_2 - E_1 E_2)$$

A fairly large degree of error comes into the application of these equations when trying to estimate emissivities. We use emissivities tabulated by White[3] which give the value for Ni plate as 0.045, the value for Al as anywhere from 0.02 for clean-polished to 0.31 for highly oxidized, and the value for Au plate as 0.026.

The heat shield is Ni plated Cu and held at a temperature of 35.5 K. The radiation incident on the heat shield is from the dewar walls which are Al and at a temperature of 300 K. The area of the dewar walls is 0.56 m^2. The following chart (Fig. 5.2) gives the radiative heat load on the heat shield for minimum, average, and maximum emissivities

Fig. 5.2 1st Stage Radiative Loading

E_1	E_2	E_{eff}	dQ/dt (W)
0.02	0.045	0.014	3.61
0.17	0.045	0.037	9.54
0.31	0.045	0.041	10.56

The second stage is Au plated and held at a temperature of 8.5 K. The radiation incident on the 2nd stage is from the heat shield which is Ni plated Cu and held at a temperature of 35.5 K. The area of the heat shield walls is 0.47 m^2. The following chart (Fig. 5.3) gives the radiative heat load on the 2nd stage.

Fig 5.3 2nd Stage Radiative Loading

| E_1	E_2	E_{eff}	dQ/dt (mW)
0.045	0.026	0.017	0.7

We see that the radiative load on the 1st stage comprises anywhere from 3.61 to 10.56 W, which could account for up to half of the 20 W that we see from the capacity map (Fig. 5.1). The load on the 2nd stage, however, accounts for only 0.7 mW and does not represent a substantial contribution to the 2W load that we see from the capacity map. While not represented on the capacity map, we should also

1. F. Reif, Fundamentals of Thermal Physics, 1965, p. 388.

2. G. K. White, Experimental Techniques in Low-Temperature Physics, 1968, p. 220.

3. G. K. White, Experimental Techniques in Low-Temperature Physics, 1968, p. 220.

consider the load on the 3rd stage. The 3rd stage receives approximately 0.7 mW, the same radiative load as the second stage. This is because the radiation incident on both stages emenates from the heat shield, and the value of T_h completely dwarfs the value of T_c in eqn. 5.1.

The next source of loading that we examine is conduction along the JT structure. The helium supplied to the JT valve travels in copper tubes which have an extremely high thermal conductivity and so facilitate heat transfer. However heat flowing in the structure must also pass through the heat exchangers. We assume that the entire temperature drop between stages occurs over the length of the heat exchanger and examine the heat flow between the two ends. The 1st stage heat exchanger is shown in Fig. 5.4.

Fig. 5.4 1st Stage Heat Exchanger
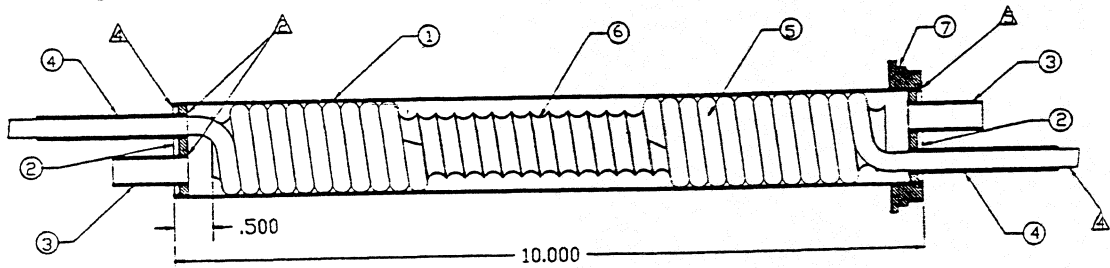
We simplify the problem of determining the heat flow across the exchanger by assuming that there are three mechanisms by which heat may flow: conduction through the outer tube (marked 1 in Fig. 5.4), through the wound bronze tubing (5), or through the inner Micarta plug (6). We assume that all of these conduction mechanisms operate in parallel so that we may simply add their contributions. This will give us an upper bound for conduction along the heat exchanger. The heat flow is given by[4]

$$(5.3) \qquad dQ/dt = A/l \, [Int_{0-Th}(\kappa(T)dT) - Int_{0-Tc}(\kappa(T)dT)]$$

where Th and Tc are the hot and cold temperatures respectively, κ is the temperature-dependant thermal conductivity, A is the cross-sectional area, and l is the length. The quantity in square brackets is referred to as the thermal boundary potential. We can now compute the heat flow through the exchanger (Fig. 5.5).

Fig. 5.5 Heat Flow in 1st Stage Heat Exchanger[5]

conduction path	material	cross-sectional area (sq. cm)	length (cm)	thermal boundary potential (W/cm)	heat flow (W)
outer tube	stainless steel	1.14	25.4	30	1.35
wound tubing	bronze	0.05	213.4	60	0.01
inner plug	Micarta	3.08	22.9	0.67	0.09

These three contributions sum to 1.45 W, with almost all of the heat being transported through the outer tube. There will be a certain amount of resistance to this heat flow in the copper tubing and this value is in effect an upper bound for the heat incident on the 1st stage due to conduction through the JT circuit. We now turn our attention to the 2nd stage heat exchanger (see Fig. 5.6), to which we

4. A. C. Rose-Innes, Low Temperature Laboratory Techniques, 1973, p. 97.

5. thermal boundary potentials for Fig. Y.5, Y.7, and Y.9 were obtained from A.C. Rose-Innes, Low Temperature Laboratory Techniques, 1973, p. 98.
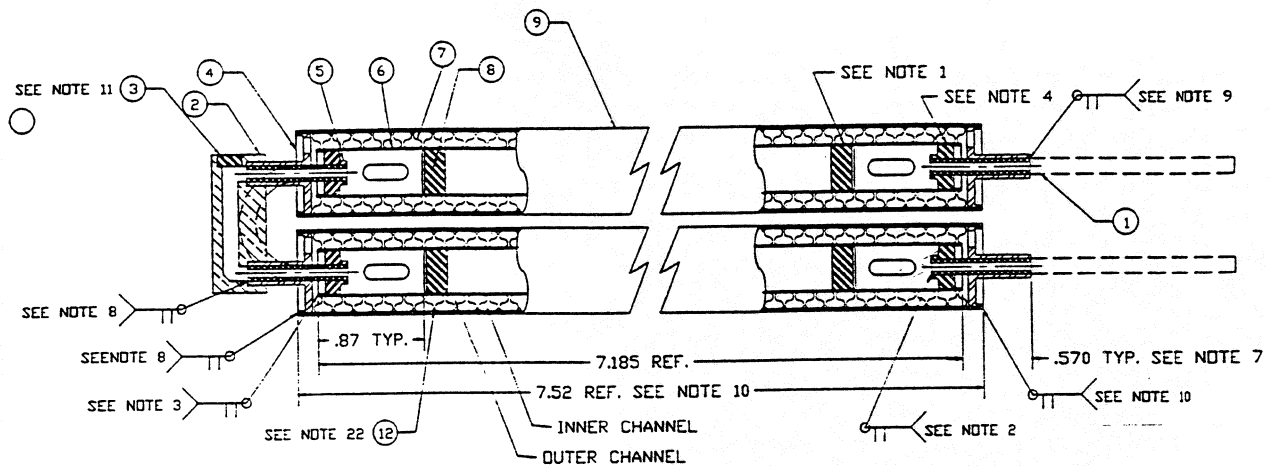
Fig. 5.8 3rd Stage Heat Exchanger

Fig. 5.9 Heat Flow in 3rd Stage Heat Echanger

conduction path	material	cross-sectional area(sq. cm)	length (cm)	thermal boundary potential (W/cm)	heat flow (mW)
outer tube	stainless steel	0.27	39.4	0.025	0.2
inner tube	stainless steel	0.08	36.5	0.025	0.1
anaconda tubing	bronze	0.01	402.6	0.088	-

We see that conduction along the 3rd stage heat exchanger amounts to only 0.3 mW. The next source of loading which we turn to is conduction along the leads. All connections to the 2nd and 3rd stages are made with cryogenic wire, along which the heat flow is negligible. However, a heater is attached to the heat shield with 2 strands of 22 gauge Cu wire. The other ends of these leads are attached to the vacuum port in the dewar wall. The wire has a radius of 0.082 cm, and travels approximately 60 cm from the dewar wall to the heat shield. Therefore, for the two strands we get a ratio of A/l of 1.07×10^{-4} cm. Once again applying eqn. 5Y.3 with a thermal boundary potential of 1000 W/cm for Cu between 35.5K and 300K, we see that the heat flow along these leads is 107 mW.

The last source of loading is from conduction in the gas, which would occur only if a proper vacuum were not obtained. Unfortunately, the vacuum gauge on our dewar only reads down to a pressure of 0.15 Pa, which we should be well below. The conduction of a gas fits into two regimes, one in which the mean free path is longer than the distance which it travels between surfaces, and the second in which the mean free path is shorter than the distance between surfaces. We are operating at a pressure significantly low to make the mean free path longer than the separation distance. In the section "Hydrogen Heat Switch" we show the conductivity in the long mean free path regime to be

$$(5.4) \qquad dQ/dt = 1/4 \ (3k/mT)^{1/2} \ paA \ (T_h - T_c)$$

where k is the Boltzmann constant, a is an accommodation coefficient ~0.5, A is the area of the hot surface, p is the pressure in Pa, T is the mean temperature, m is the mass of a He molecule, and T_h and T_c are the hot and cold temperatures respectively. We would like to evaluate this equation to find when the gaseous conduction is negligible (Fig. 5.10). We see that the conduction is negligible as high as 1.5 mPa (or 11.3 µtorr), and in fact pressures as low as 0.15 mPa (or 1.1 µtorr) should be attainable.

Fig. 5.10 Gas Conduction on 1st and 2nd Stages

pressure (mPa/torr)	dQ/dt (mW) on 1st Stage	dQ/dt (mW) on 2nd Stage
0.15 / 1.13e-6	3.29	0.55
0.75 / 5.63e-6	16.43	2.73
1.50 / 1.13e-5	32.88	5.45
15 / 1.13e-4	328.96	54.56

We are unable to explain the full 20 W first stage and 2 W 2nd stage load that we see in Fig. 5.1. We see that radiation may be responsible for as much as 10.56 W on the 1st stage and 0.7 mW on the 2nd stage, conduction in the JT circuit may be responsible for as much as 1.45 W on the 1st stage and 10.2 mW on the 2nd stage, and conduction along leads may be responsible for 0.11 W on the 1st stage. We assume that gas conduction is negligible. This still leaves a load of 7.88 W on the 1st stage and practically the whole 2nd stage load of 2 W unaccounted for. In addition, we see that the 3rd stage is subject to no significant loads from the sources examined.

6. Balzers Model UCH 130 Parameters

The performance of the refrigerator may be affected by adjusting the parameters of the Balzers Model UCH 130 Refrigerator. These include input pressure and cycle frequency, and we examine them each in turn. The work, W, done by a gas upon expansion is given by

(6.1) $W = Int (p \, dV)$

where p is the pressure, V is the volume, and Int is the integral from V_i to V_f. This can be visualized as the area under the curve between V_i and V_f on a pressure vs. volume diagram for the system (Fig. 6.1).

Fig. 6.1 Pressure vs. Volume Diagram for Gas Expansion[1]
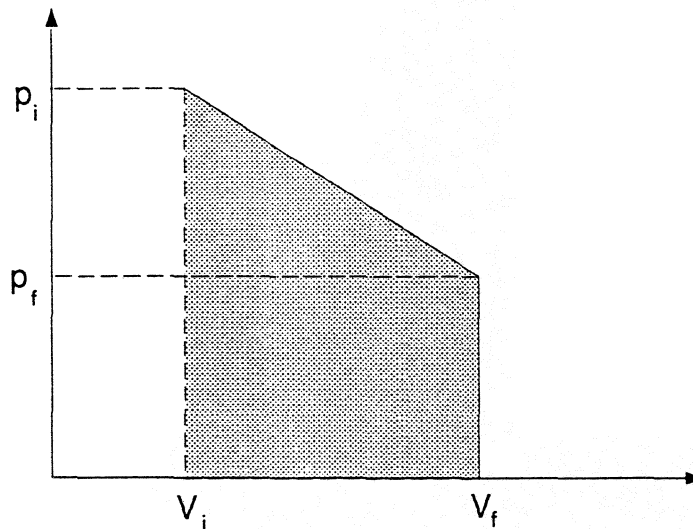
In our case p_i and p_f are the supply and return pressures to the Balzers unit, V_i is the gas volume in the refrigerator, and $V_f - V_i$ is the gas volume in the compressor. It should be clear that increasing the input pressure is one way to make the gas do more work, therefore providing more cooling capacity. Experiment bears out this expectation as we recorded the 1st, 2nd, and 3rd stage temperatures of the refrigerator while varying the input pressure to the Balzers unit (Fig. 6.2). For these trials, the JT pressure was kept at 1930 kPa, and the Balzers cycle frequency at 144 r.p.m.

---

1. Fig. Q.1 does not intent do imply that pressure must be linearly dependant on temperature

## Fig. 6.2 Dependence of Temperature on Balzers Pressure
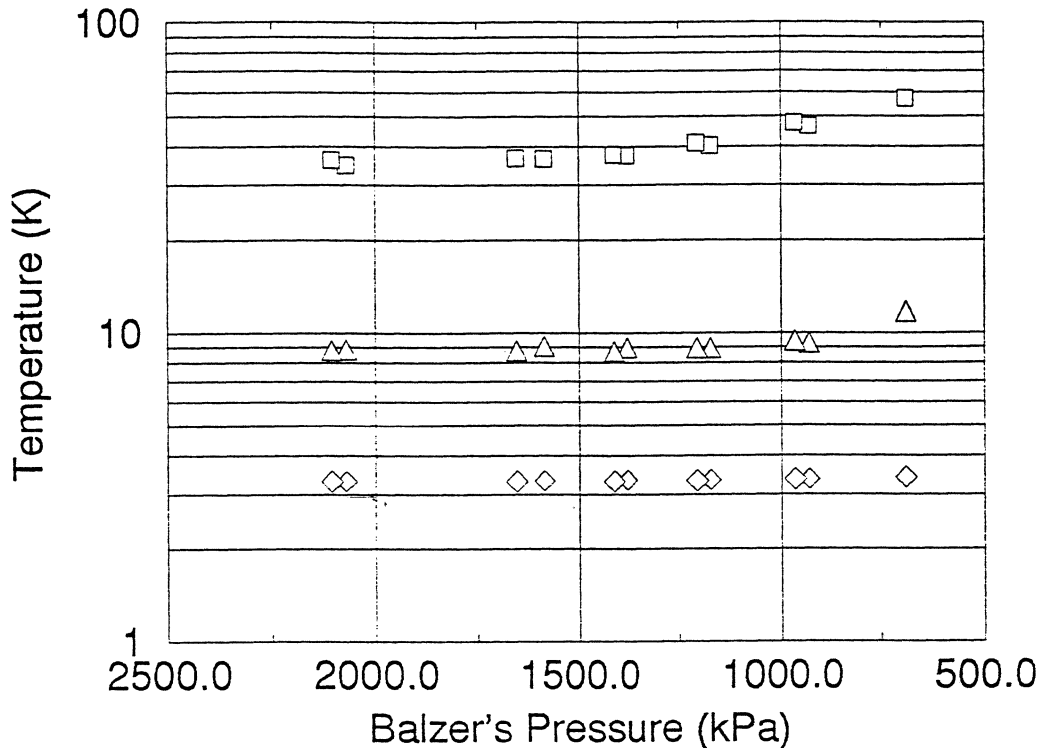
The interesting thing to note about Fig. 6.2 is that the temperatures do not follow a linear dependence on pressure, but in fact remain relatively constant down to 1379 kPa on all stages. However, a load test at 1379 kPa showed the refrigerator to have a capacity of only 1W with a 50 W load on the 1st stage and a 2W load on the 2nd stage. While this is not a sufficient capacity for our purposes, more testing in the 1379 to 2069 kPa range may show that the refrigerator can be operated at a pressure below 2069 kPa while retaining the major part of its capacity. This is desirable because running the refrigerator at a lower pressure would mean a reduction in energy costs.

The control unit for the Balzers Model UCH 130 refrigerator allows the cycle frequency to be adjusted from 56 - 144 rpm. We performed tests covering the entire range of frequencies and found that the temperature of the refrigerator's 2nd stage decreases with increasing frequency (Fig. 6.3). This is what we would expect since the more cycles that the refrigerator performs in unit time, the more heat it removes in this time, resulting in a lower temperature. However, it only works this way because our refrigerator is always subject to some load. Notice that the differences between the temperatures at low and high frequencies decrease as the load on the refrigerator is reduced. Even with the JT valve off, our refrigerator is still subject to loads of 20 W on the 1st stage and 2 W on the 2nd stage. Were we able to eliminate this load, we would expect the slope of the curve to change, and the temperature to be the lowest at the smallest frequencies[2].

2. as found by R. Plambeck, N. Thatte, and P. Sykes, *A 4K Gifford-McMahon Refrigerator for Radio Astronomy*, presented at 7th International Cryocooler Conference, Santa Fe, NW, 1992, p. 7.

Fig. 6.3 Dependence of Temperature on Balzers Cycle Frequency
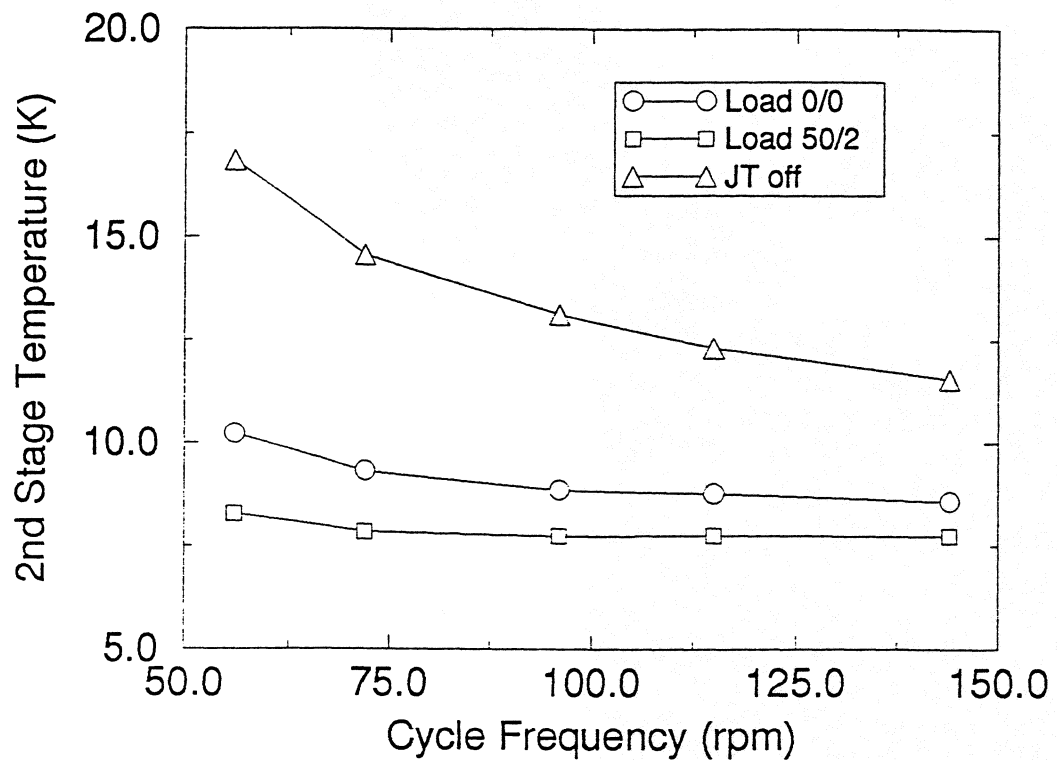
In conclusion, it is possible that reducing the input pressure to the Balzers is a significant way of improving refrigerator efficiency. However, more tests need to be done in the specified pressure range in order to confirm this. Due to the relatively large loads that our refrigerator will be subject to during operation, reducing the cycle frequency on the Balzers control unit is not advised. Only with very little loading on the refrigerator is this worthwhile.

7. Hydrogen Heat Switch

Thermal coupling between the 2nd and 3rd stages in the refrigerator is provided by a hydrogen gas-gap thermal switch. It is useful to take a look at the heat switch for two reasons. The first is that conduction across the switch from the 8.5K 2nd stage to the 3.5K 3rd stage represents a possible source of heat loading on the 3rd stage. The second is that through better understanding how the heat switch works, we can hope to design them more efficiently. The switch consists of two OFHC Cu tubes mounted one inside of the other and held together by a stainless steel shell (see Fig. 7.1). The switch is filled to 690 kPa with H_2 gas at room temperature. We can trace the response of the switch pressure to temperature on a phase change diagram (see Fig. 7.2).

Fig. 7.1 Hydrogen Heat Switch
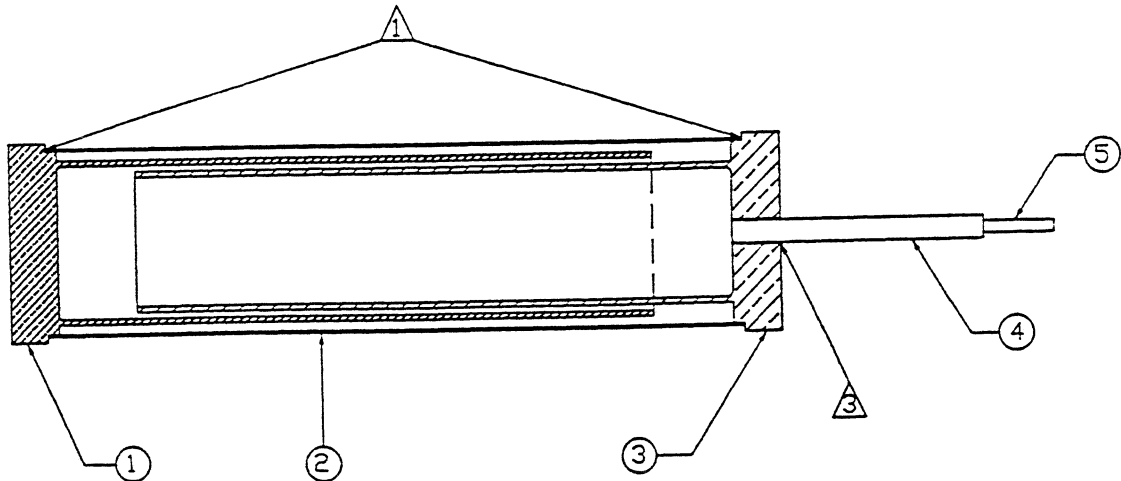
The dashed lines marked 690 kPa in Fig. 7.2 show what happens as the temperature is lowered from room temperature. The lower of the two curves represents the dependence of pressure on temperature as given by the Van-der-Waals equation[1]

$$(7.1) \qquad (V - nb)(p + an^2/V) = nRT$$

where V is volume, n is the number of moles, p is the pressure, R is the ideal gas constant, T is the temperature, and a and b are constants which depend on the particular gas. The upper of the two curves represents the dependence of pressure on temperature as given by the ideal gas law
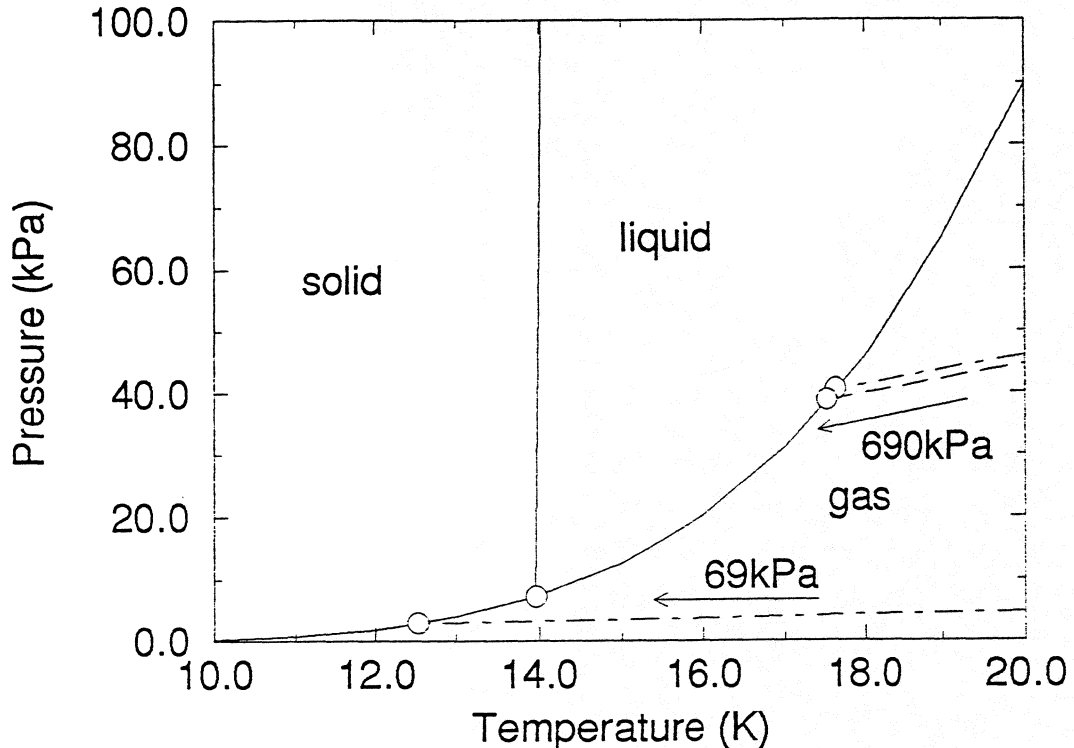
$$(7.2) \qquad pV = nRT$$

The curve from the Van-der-Walls equation is a closer approximation to the behavior of a real gas, but

1. P. W. Morse, Thermal Physics, 1969, p. 25.

both methods give approximately equal results. Due to its ease of use, we will use the ideal gas law for all subsequent calculations.

Fig. 7.2 Phase Change Diagram[2] for H_2

The point at which the curves marked 690 kPa intersect the gas/liquid boundary in Fig. 7.2 marks where a portion of the gas in the switch condenses. As soon as there is some liquid present in the heat switch, the pressure in the switch is governed by the vapor pressure of the gas. Since the condensate will form on the cold end of the switch, the pressure in the switch will be entirely governed by this temperature. This vapor pressure curve can be fit empirically by[3]

(7.3) $\log(p) = 6.74932 - 47.0172/T + 0.03635T$

where p is in Pa, and T is the temperature of the cold end of the switch. The most important result of this is that the switches do not need to be filled to a pressure of 690 kPa at room temperature, as the following calculation will show.

The thermal conductivity of the hydrogen gas in the switch depends on whether the mean free path of the gas is longer or shorter than the separation distance between the copper tubes. The mean free path, l, is given by[4]

(7.4) $l = 1/N\sigma$

2. data for the vapor pressure of H_2 are taken from H.W. Wooley, R. B. Scott, and F. G. Brickwedde, *J. Research NBS* 41, 1948, p. 379.

3. H. W. Woolley, R. B. Scott, and F. G. Brickwedde, *J. Research NBS* 41, 1948, p. 379. It is important to note that this equation is an emperical relation based on data taken above 9K. It may or may not be accurate at temperatures below that point.

4. P. W. Morse, Thermal Physics, 1969, p. 175.

where N is the molar density and σ is the collision cross section. This is equivalent to[5]

$$(7.5) \qquad l = kT/\pi s^2 p$$

where k is the Boltzmann constant, s is the effective molecular diameter[6], and p is the function of cold-end temperature given by eqn. 7.3. Setting the mean free path, l, equal to the separation distance between the two tubes, d, we find that

$$(7.6) \qquad \log(d\pi s^2/k) = \log(T) - 6.74932 + 47.0172/T - 0.03635T$$

This equation can be solved numerically for values of d = 1.68 mm and s = 2×10^{-10}m to show that the mean free path is equal to the separation distance at T = 6.4 K (see Fig. 7.3).

Fig. 7.3 Mean Free Path of H_2
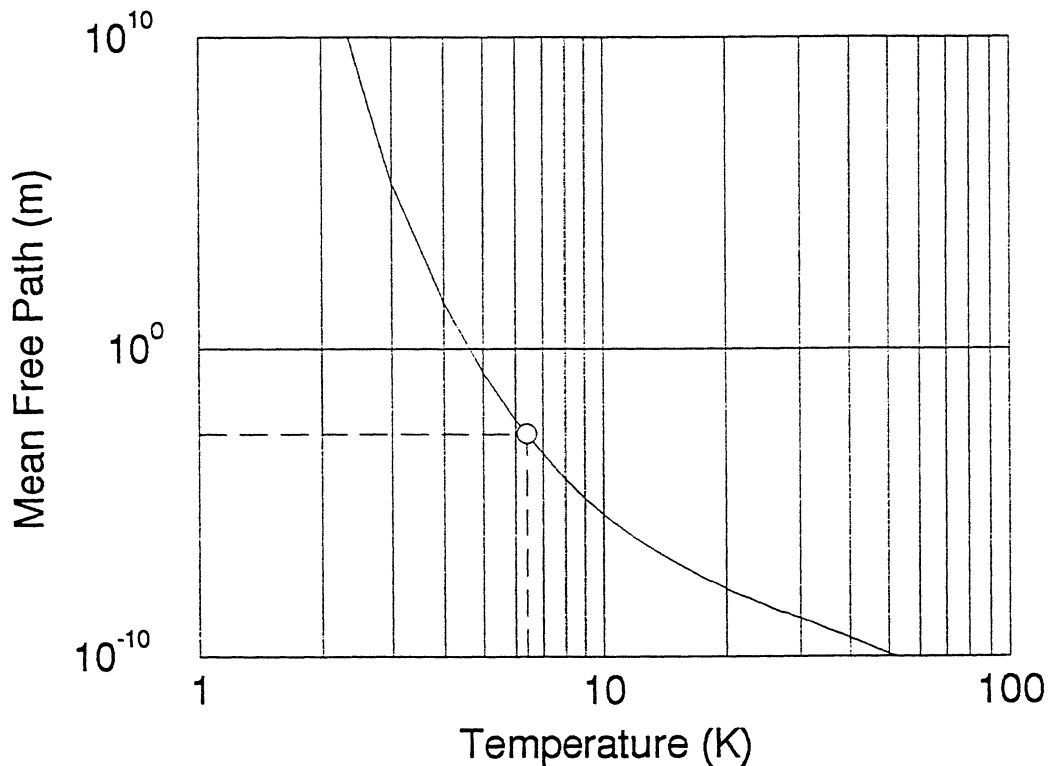
When the mean free path, l, is less than the separation distance, d, i.e. for temperatures greater than 6.4 K, the conductivity of the gas, κα, is given by[7]

$$(7.7) \qquad \kappa\alpha = Nvcl/3$$

where c is the specific heat per molecule (equal to 5k/2 for a diatomic molecule[8]) and v is the mean

5. note that F. Reif, Fundamentals of Statistical and Thermal Physics, 1965, p. 471, gives "l=kT/2^{1/2}πs^2p" as a more correct form of this equation. However, this form does not agree as well with experimental data as given by A. C. Rose-Innes, Low Temperature Laboratory Techniques, 1973, p. 237.
6. a typical value for the molecular diameter of 2×10^{-10}m is given by F. Reif, Fundamentals of Statistical and Thermal Physics, 1965, p. 471.
7. F. Reif, Fundamentals of Statistical and Thermal Physics, 1965, p. 481.
8. F. Din and A. H. Crockett, Low Temperature Techniques, 1960, p. 128.

gas particle velocity. The mean gas particle velocity is found to be[9]

$$(7.8) \qquad\qquad v = (3kT/m)^{1/2}$$

where m is the mass of an H_2 molecule and from the ideal gas law, the molar density is given by

$$(7.9) \qquad\qquad N = p/kT$$

Substituting these quantities into eqn. 7.7, we find that

$$(7.10) \qquad \kappa\alpha = 5k/6\pi s^2 \, (3kT/m)^{1/2} = (1.02 \times 10^{-4} W/K^{3/2}cm) \, T^{1/2}$$

The important thing to notice about this is that the conductivity is independent of pressure. That means that, regardless of what pressure the switch is initially filled to, the thermal performance of the switch will be the same as long as the pressure in the switch intersects the vapor pressure curve at a temperature above 6.4 K.

We can find to what pressure the heat switch must be filled at room temperature in order to intersect the vapor-pressure curve at above 6.4 K. From Eq. 7.3, the pressure of the gas at 6.4 K is 0.43 Pa. Assuming the ideal gas law

$$(7.11) \qquad\qquad P_{cold}/T_{cold} = P_{hot}/T_{hot}$$

we see that at room temperature, the switch must be filled to a pressure of at least 22 Pa, in order to intersect the vapor-pressure curve at this point.

Agreement of our theory with experimental results obtained by Balister[10] is shown in Fig. 7.4. The cold end of the switch was held fixed at 20 K so that we are in the l < d regime. The circles show the experimental data, and the solid curve is the theoretical curve derived from eqn. 7.10. The percentage of error ranges from 27 to 53% over the temperature range, with our values consistently lower than the experimental data. While we have only plotted the values due to conduction in the gas, there is also conduction along the stainless steel outer shell, approximately 0.03 W in this range. This reduces the discrepancy to 21% at the low end of the temperature range. It is important to realise how much error is associated with a calculation of this type. Specific heat is not a constant, but in fact varies with both temperature and pressure, and the effective diameter must be estimated as experimental data is unavailable in this temperature range. Factors such as this most likely compose the majority of the error in the calculation.

9. P.W. Morse, Thermal Physics, 1969, p. 170.
10. M. Balister, Hydrogen Switch, 1981, p. 5.

Fig. 7.4 Heat Flow in the Short Mean Free Path Regime
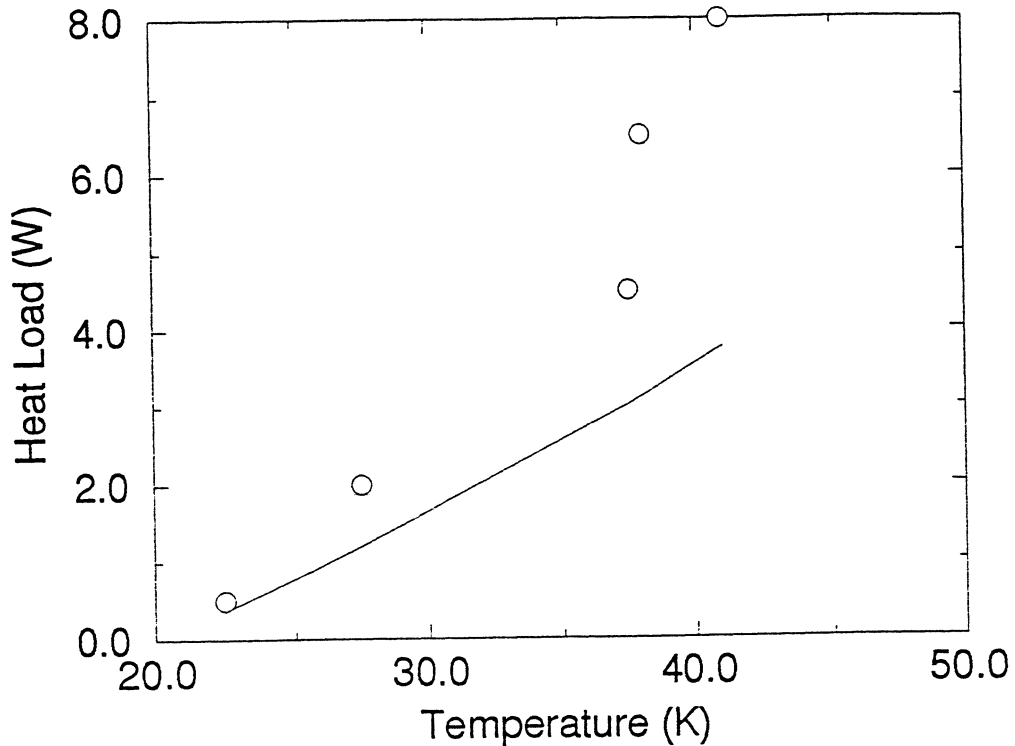
We would also like to understand the thermal conduction mechanism when the mean free path, l, is greater than the separation distance, d. Consider two plates held at a fixed distance, d, from eachother and held at two different temperatures T_C and T_H (Fig. 7.5).

Fig. 7.5 Parallel Plate Gaseous Conduction
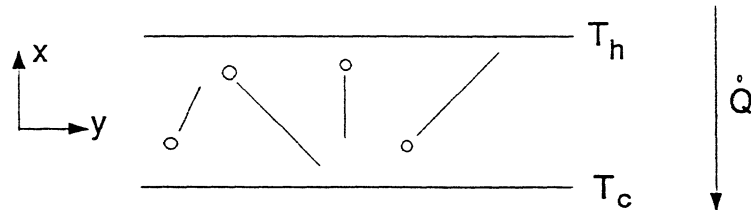
Since the mean free path is longer than the separation distance, d, the average molecule moves from one plate to the other without hinderance. Thermodynamic principles prohibit all of the molecules from stacking up on one side, and so the number of molecules travelling in either direction must be the same. Consider a molar volume of N molecules. Approximately 1/3 of these are moving in the x direction. Of these, approximately half are moving in the positive x direction, and half in the negative x direction. This means that Nv/6 molecules strike either side in unit time[11].

Each molecule carries kinetic energy given by

(7.12) $E = 1/2mv^2$

where m is the mass of the molecule and v is the mean velocity. The mean velocity in turn, is found

11. F. Reif, Fundamentals of Statistical and Thermal Physics, 1965, p. 474.

from the equipartition of energy to be

$$(7.13) \qquad\qquad v = (3kT/m)^{1/2}$$

where k is the Boltzmann constant and T is the temperature of the surface away from which the molecule is travelling. Substituting this into the expression for energy we see that

$$(7.14) \qquad\qquad E = 3kT/2$$

From above, we know that $Nv/6$ molecules must strike each side in unit time. Subtracting the energy carried away from T_C from that carried towards T_C, and multiplying by the surface area we see that

$$(7.15) \qquad\qquad dQ_\beta/dt = ANvk/4 \; (T_H\text{-}T_C)$$

where A is the area of either surface. Since heat flow in general is given by

$$(7.16) \qquad\qquad dQ_\beta/dt = A/d \; \kappa \; (T_H\text{-}T_C)$$

where d is the distance between the hot and cold surfaces, and κ is the thermal conductivity of the material, we see that the thermal conductivity of the gas is

$$(7.17) \qquad\qquad \kappa_\beta = Nvkd/4$$

In order to compute heat flow from this, one does not use a normal conductivity integral, but instead simply multiplies the conductivity by the geometrical term and the temperature difference between the two plates.

Note, this equation should also include an accomodation coefficient which governs the amount of energy that the molecule is able to transfer to the plate upon collision. This coefficent, which must take on a value somewhere between 0 and 1, is a significant source of eror as it is extremely hard to estimate. A good value for hydrogen gas incident upon OFHC Cu might be ~0.5.With this included the conductivity becomes

$$(7.18) \qquad\qquad \kappa_\beta = aNvkd/4$$

where a is the accommodation coefficient. Substituting values derived above we find that

$$(7.19) \qquad \kappa_\beta = d/8 \; (3k/m)^{1/2} \; p/T^{1/2} = (2.34\text{x}10^{-4} \; W/K^{1/2} \; cmPa) \; p/T^{1/2}$$

We now see why it is important that we intersect the vapor pressure curve at above 6.4 K as the thermal performance below this point is strongly dependant on pressure.

The conductivity in this regime does not at all agree with data obtained by Balister[12] for

12. M. Balister, *Hydrogen Switch*, 1981, p. 4.

performance of the switch in this regime. With the cold stage temperature fixed at 4.2K, we would expect the heat flow to be kept under 1 mW for hot stage temperatures up to 50K. However, Balister found heat flow as high as 360 mW in this range. We can attribute only 40 mW of this to heat flow in the stainless steel. The most likely cause of this error is that we are using a pressure function which drops off rapidly at temperatures less than 10 K, and has not been shown to be accurate in this range.

We can use these two conductances to find the heat that flows between the cylinders. In the first regime, we may think of the gas as forming a temperature gradient between the two cylinders, and can then evaluate the heat flow as a thermal conductivity integral across this temperature gradient. We make the assumption that there is no drop in temperature along the copper cylinder because of its high thermal conductivity, and can then write

$$(7.20) \qquad\qquad dQ_\alpha/dt = A/d \ Int(\kappa_\alpha \ dT)$$

where A is the surface area of the inner conducutor, d is the separation distance between the tubes, κ_α is as defined in eqn. 7.10, and Int is the integral from 8.5K to T. This curve is plotted as the dot-dash line in Fig. 7.6.

When l>d, we do not have a temperature gradient because in this regime each molecule of gas travels from one surface to the other without colliding with any other molecules. From the derivation above, we see that the proper way to evaluate the heat flow is by

$$(7.21) \qquad\qquad dQ_\beta/dt = A/d \ \kappa_\beta \ (T_2-T_3)$$

where T_3 and T_2 are the 3rd and 2nd stage temperatures respectively and κ_β is as defined in eqn. 7.19. These values are plotted as the solid curve in Fig. 7.6, with T_2 fixed at 8.5K.

Fig. 7.6 Heat Flow Across Hydrogen Heat Switch
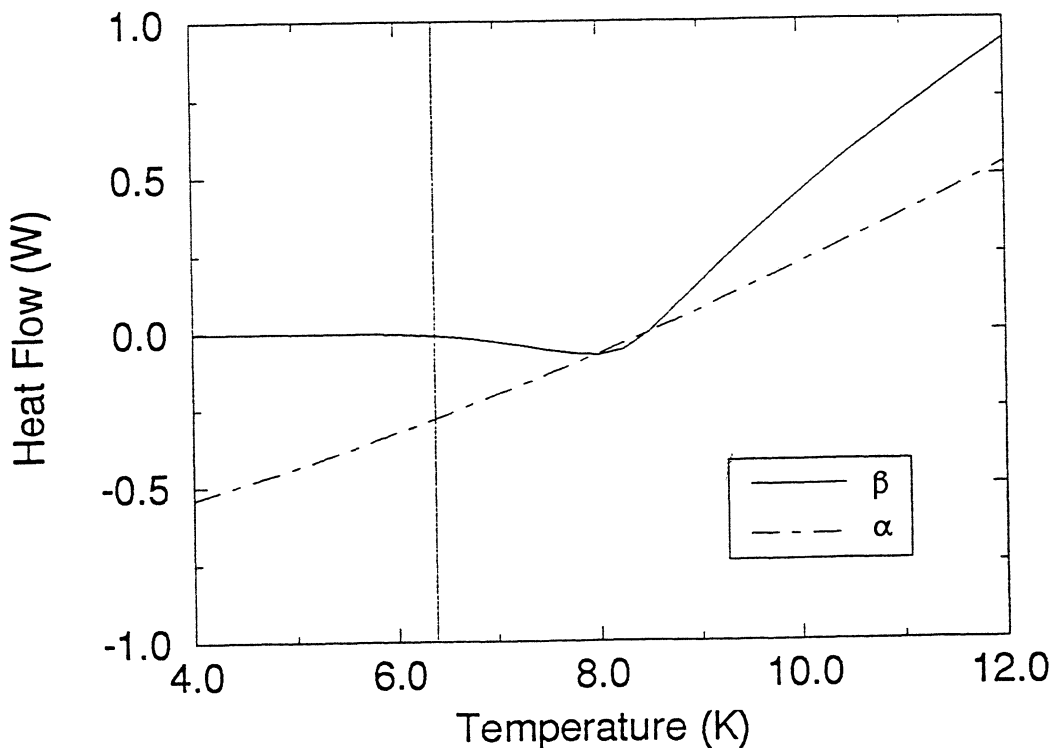
We see that at very low temperatures, almost no heat is flowing through the gas. This means that heat conduction in this regime will be effectively governed by the stainless steel outer shell of the heat switch. The heat flow due to the stainless steel is ~1 mW at these temperatures. From Fig. Z.3, we know that we expect the transition between the two regimes to occur at approximately 6.4 K (marked by the solid vertical line in Fig. 7.6). Also, from Fig. 7.3 we see that moving to either side of this point by 1 K increases the mean free path by more than a factor of ten, landing us well into one or the other of the regimes. However, what happens at the transition point we are unsure of, and so have represented the conductivity from both regimes about this point in Fig. 7.6.

We now return to the original question, which was whether or not conduction across the heat switch is a significant source of 3rd stage loading. We see (Fig. 7.6) that with a 2nd stage temperature of 8.5K and a 3rd stage temperature of 3.5K, there is practically no heat is flowing through the gas, and the heat flow will be entirely through the stainless steel, ~1 mW. In conclusion, the hydrogen thermal switch is not a concern in thermal loading. Even if we are to beleive the data obtained by Balister, we would only expect a heat load of ~5 mW on the 3rd stage, which is still not a concern.